

# Magnetic Nanowires in Hexagonally Ordered Pores of Alumina

Robert M. Metzger, Valery V. Konovalov, Ming Sun, Tao Xu, Giovanni Zangari, Bin Xu, Mourad Benakli, and W. D. Doyle, *Fellow, IEEE*

**Abstract**—Acid-anodized aluminum forms amorphous alumina with long and columnar nanopores with approximately hexagonal ordering (“alumite”). Excellent hexagonal ordering of these nanopores has been achieved by 24 hours of anodization, but with restricted domain size ( $2\text{--}4\ \mu\text{m}^2$ ), which can be increased to  $100\ \mu\text{m}^2$  with longer anodization. We have deposited Fe in disordered pores and Co in ordered pores; we can control the average length and diameter of these nanowires, but there is still a distribution of nanowire lengths. Previously, we described Fe nanowires with diameters down to 11 nm in disordered pores. Here we focus on longer (770 nm) and shorter (64 nm) Co nanowires with diameters of 25 nm in ordered pores with 100 nm pore-to-pore separation. The longer wires have an easy axis out-of-plane, with squareness  $>0.9$ , coercivity = 1900 Oe, and a fluctuation field of 5.3 Oe. The shorter wires are more isotropic, with lower coercivities ( $\approx 1300$  Oe) and larger fluctuation fields  $\approx 8.4$  Oe.

**Index Terms**—Alumite, anodized aluminum, cobalt nanowires, coercivity, extra-high density magnetic recording, fluctuation field, iron nanowires, nanopores, perpendicular magnetic recording, squareness.

## I. INTRODUCTION

THE THERMAL stability limit for magnetic recording density in conventional longitudinal recording may be  $<50\ \text{Gb in}^{-2}$  [1], but more recent calculations are more optimistic [2]. Linear density limits are currently determined by the medium noise. The power signal-to-noise-ratio (SNR) is determined by the number of grains which constitute the single bit. For a fixed bit size, the number of grains and the SNR could be increased by decreasing their dimensions, but this approach is limited by the thermal stability of the written magnetization transition, which is mainly determined by the demagnetizing fields and by the energy barrier to magnetization reversal for a magnetic grain. This limit could be relaxed to the superparamagnetic limit for the material of interest, if a bit cell consisted of a single and isolated magnetic unit. Such an ideal magnetic medium would consist of ferromagnetic islands

of nm dimensions, placed in an ordered fashion on the sites of a nm-sized 2-dimensional lattice (magnetic array). Current approaches to such magnetic arrays employ e-beam lithography to define the array geometry [3]–[5].

Anodization of aluminum is a much cheaper process for the synthesis of a nm-scale porous structure, consisting of close-packed cells in a local hexagonal arrangement, with pores at their centers. Hexagonally ordered patterns on micrometer-sized domains can be obtained by cycles of anodization and successive removal of the porous oxide. Such a method appears very promising for the production of hexagonal patterns with extended long-range order. Magnetic materials can be electrodeposited into these pores by AC electrodeposition [6], producing isolated needle-like particles which have been of interest for perpendicular magnetic recording. The implication for magnetic recording is that an ordered perpendicular (or longitudinal) medium should exhibit much lower noise, compared to a disordered medium, thus increasing the signal-to-noise ratio [7], although this has been debated [8]. The nanowires that can be introduced into the pores by electrodeposition may potentially produce bit densities in excess of  $100\ \text{Gbit in}^{-2}$ .

The controlled anodization of aluminum has been an industrial process since the 1920's [9], but the main emphasis was anodization at pH above 7, to yield thick corrosion-resistant passivated oxide “barrier type films.” When Al is anodized in acidic solutions, pores form which have only an approximately hexagonal order [10], which is idealized as truly hexagonal in Fig. 1: this structure has been called “alumite” [6]. Since the pores were relatively uniform (Fig. 2), their use as hosts for magnetic nanowires of Fe or Co received early attention by many groups worldwide [6], [11]–[15], including our own [16]–[18]. The mechanism for pore formation and its hexagonal ordering (a mesoscopic phenomenon) remains unknown. Early interest by the hard disk industry in magnetic nanowires in alumite faded in the early 1990's.

Since then, a dramatic breakthrough was achieved when Masuda and co-worker showed that prolonged anodization, followed by stripping of the thick oxide, and re-anodization produced ordered nanopores with perfectly hexagonal domains [19]. This result was confirmed by us [20], [21] (Fig. 3), and by others [22], [23].

The Al surface is usually flattened before anodization by an initial electropolishing step, which removes some of the “hills” in the sample, and may leave local thin spots in the air-formed oxide layer [21]. Ordering within this electropolishing step has received experimental [24] and theoretical [25], [26] attention: ordered patterns of small hillocks or stripes (not pores) can

Manuscript received August 19, 1999. This work was supported by DOD-URISP-DAA-H04-96-1-0316 and by NSIC-NSF-EHDR-542417-55139.

R. M. Metzger, V. V. Konovalov, M. Sun, and T. Xu are with the Department of Chemistry and the Center for Materials for Information Technology, University of Alabama, Tuscaloosa, AL 35487-0336 U.S.A. (e-mail: rmetzger@bama.ua.edu).

G. Zangari is with the Department of Metallurgical and Materials Engineering and also the Center for Materials for Information Technology, University of Alabama, Tuscaloosa, AL 35487-0202 U.S.A. (e-mail: gzan-gari@coe.eng.ua.edu).

B. Xu, M. Benakli, and W. D. Doyle are with the Department of Physics and the Center for Materials for Information Technology, University of Alabama, Tuscaloosa, AL 35487-0209 U.S.A. (e-mail: wdoyle@magnet.mint.ua.edu).

Publisher Item Identifier S 0018-9464(00)00707-X.

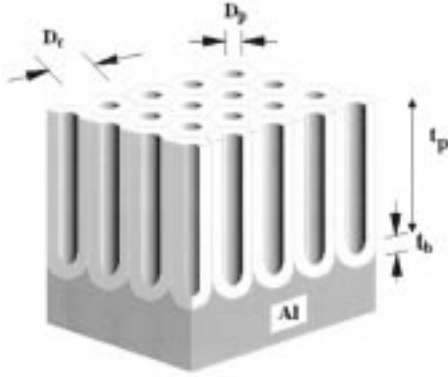


Fig. 1. Idealized hexagonal array [10] of porous  $\text{Al}_2\text{O}_3$  film formed by DC anodization of Al in acid (sulfuric, oxalic, or phosphoric, below pH 4).  $D_p$  ( $=11$  to  $100$  nm), is the pore diameter;  $D_c$  ( $=30$  to  $150$  nm) is the spacing between the pores;  $t_b$  ( $\approx 10$  nm) is the thickness of the barrier-type film at the bottom of each pore,  $t_p$  ( $=0$  to hundreds of  $\mu\text{m}$ ) is the length of the pore. Both  $D_p$  and  $D_c$  have very narrow distributions, selectable by controlling the pH and the anodization voltage. As anodization proceeds, the Al metal is consumed, and the pore length  $t_p$  increases, while  $t_b$  stays constant.

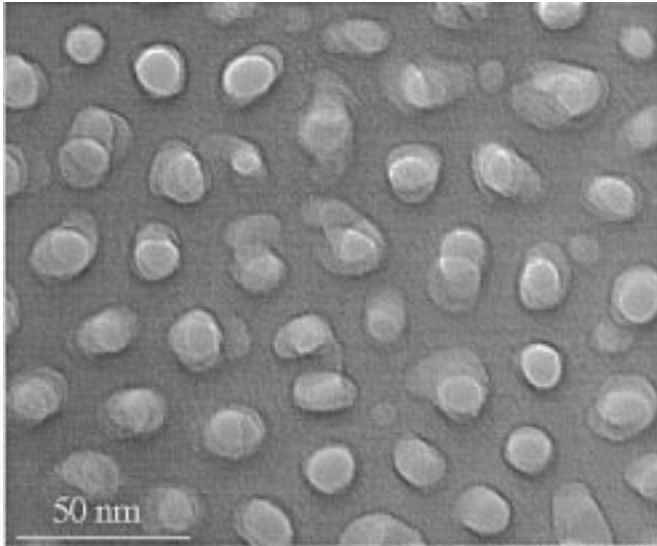


Fig. 2. TEM top view of disordered alumite film formed in 15%  $\text{H}_2\text{SO}_4$  [18].

be observed. Stripes can extend throughout the sample when a single crystal Al (110) substrate is used [27]. Ordered hills or stripes are also seen when an Al sample is heated for a long time within  $50^\circ\text{C}$  of its melting point [28].

We review here the synthesis of highly ordered hexagonal patterns on mesoscopic scales, and the electrodeposition of Co magnetic arrays with thickness of interest for magnetic recording; we summarize our published results [16]–[18], [21], [27] and report on recent progress in extending the ordered domains, probing the mechanism for ordering, to prepare Co nanowires, and analyzing their magnetic properties.

## II. ELECTROPOLISHING AND PATTERN FORMATION ON Al

Electropolishing is an essential step for forming ordered hexagonal patterns [22]. Other patterns are also formed during electropolishing [24], [25]. Using single-crystal Al (110) samples, stripes (1–7 nm high, with repeat distances of  $42 \pm$

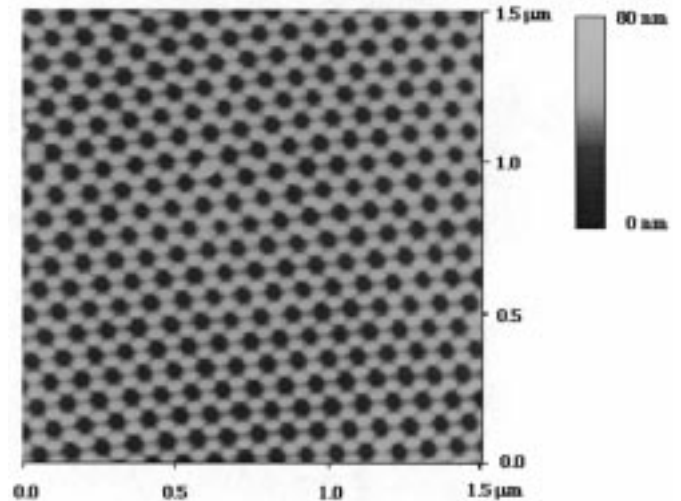


Fig. 3. Atomic force micrograph ( $1.5 \times 1.5 \mu\text{m}^2$ ) of ordered aluminum Al (plus  $\text{Al}_2\text{O}_3$  formed in air) after anodizing in  $\text{H}_2\text{C}_2\text{O}_4$  for 25 hours, then stripping  $\text{Al}_2\text{O}_3$  porous film with  $\text{H}_3\text{PO}_4/\text{H}_2\text{CrO}_4$ . The darker spots are the pore bottoms. From [21].

2 nm at 20 V DC and  $62 \pm 2$  nm at 40 V DC) were found to extend uniformly throughout a  $1 \text{ cm}^2$  sample [27]: this was true macroscopic ordering. A detailed theory explains when stripes, hexagonal mounds, or unstable patterns appear, by implicating the adsorption of alcohols on the surface [25], [26]; this theory may not apply to hexagonally ordered nanopores, whose periodicities only share the same order of magnitude as the structures formed by electropolishing.

## III. ANODIZATION IN ACIDS: DISORDERED PORES

The recipe for forming porous structures in Al by anodizing in acid is simple. Using pure Al (or even the Al–1% Mg alloy used for commercial soda cans, but not commercial Al plate [16]), acids such as  $\text{H}_2\text{SO}_4$ ,  $\text{H}_2\text{C}_2\text{O}_4$ ,  $\text{H}_3\text{PO}_4$ , or  $\text{H}_2\text{CrO}_4$  (but not HCl) and a DC power supply, prolonged anodization (e.g., for a  $3 \text{ cm}^2$  Al surface, a Pb or Al cathode, in 3%  $\text{H}_2\text{C}_2\text{O}_4$  or 4%  $\text{H}_3\text{PO}_4$  at potentials between 10 and 60 V DC) creates a porous structure (Fig. 2) that only crudely resembles the structure depicted in Fig. 1. The pore growth rate is  $0.1 \mu\text{m min}^{-1}$ . Amorphous and anhydrous  $\text{Al}_2\text{O}_3$  forms, but the pore bottom of  $\text{Al}_2\text{O}_3$  may be partially crystalline. The reaction at the metal/oxide interface (anode) is  $\text{Al} \rightarrow \text{Al}_{\text{oxide}}^{+++} + 3e^-$ ; the probable reaction at the pore bottom/electrolyte interface is water splitting:  $2 \text{H}_2\text{O} \rightarrow \text{O}_{\text{oxide}}^{--} + \text{H}_3\text{O}^+$ ; the reaction at the cathode is hydrogen evolution:  $2 \text{H}_3\text{O}^+ + 2e^- \rightarrow 2 \text{H}_2\text{O} + \text{H}_2$ . For polybasic acids, the side walls of the pores contain some  $\text{HSO}_4^-$ ,  $\text{HC}_2\text{O}_4^-$ , or  $\text{HPO}_4^{--}$ : the acid equilibria probably compete with the water-splitting reaction. Within 10 s of anodization, the pore bottoms become highly resistive ( $10 \text{ M}\Omega \text{ cm}^{-2}$  [30]). Thereafter, the current increases about five-fold and remains steady over time, as pores form, until the Al is exhausted.

The pore spacing  $D_c$  is independent of the electrolyte and pH, and is about  $2.8 \text{ nm V}^{-1}$ , where  $V$  is the applied voltage [29]. The pore diameter  $D_p$  varies somewhat with acid, concentration, and temperature: the  $D_c/D_p$  ratios are 1.74 to 2.15 for  $\text{H}_3\text{PO}_4$ , 3.33 for  $\text{H}_2\text{CrO}_4$ , 4.88 for  $\text{H}_2\text{SO}_4$ , and 3.01 for  $\text{H}_2\text{C}_2\text{O}_4$  [29].

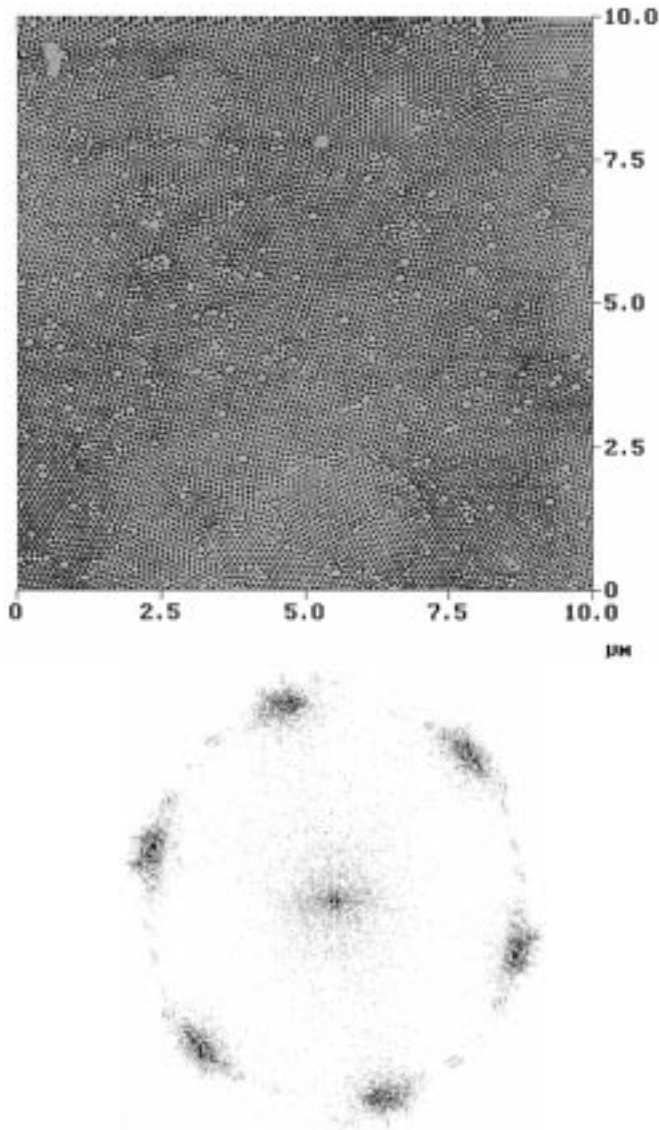


Fig. 4. AFM ( $10 \times 10 \mu\text{m}^2$ ) of Al after 87 h of anodization and removing the oxide, as in Fig. 3 (left). 2-D Fourier transform of AFM (right).

It was originally suggested that the pores initiated at cracks or other defects in oxide initially produced during anodization [31]. It appears, however, that any process that thins the oxide locally can initiate pore formation.

#### IV. ANODIZATION IN ACIDS: ORDERED PORES

Masuda and Fukuda achieved a truly hexagonal ordered pattern by first electropolishing (to eliminate the major “mountains” in the substrate), then anodizing for 24 hours, then stripping off the oxide (in 0.2 M  $\text{H}_2\text{CrO}_4$  and 0.4 M  $\text{H}_3\text{PO}_4$  at  $60^\circ\text{C}$ ), and finally anodizing again for a relatively short time [19]. We have produced similar results (Fig. 3) [21]: we can form hexagonal domains with a domain size of 2 to  $4 \mu\text{m}^2$  [21]. By extending the anodization to 87 h, we have found domains of between 10 and  $100 \mu\text{m}^2$  (Fig. 4), but the defects at the grain boundaries become deeper [32]. To obtain macroscopic ordering in alumite, one can nanoindent an electropolished Al substrate with a Si template prepared by electron beam lithography to produce small concavities at the

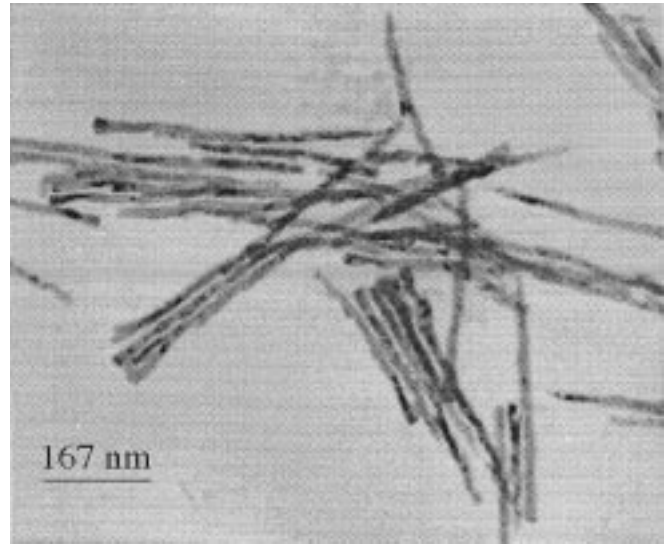


Fig. 5. TEM micrograph of  $\alpha$ -Fe particles freed from the alumite film [18].

“right” spacing, then anodizing at the voltage and pH needed for pore growth at that spacing [33].

Electropolishing is essential for ordered pore growth [23]; etch pits, local stresses, or locally thinner oxide may initiate pore growth. A kinetic theory for single pore growth was presented [34], [35], but no satisfactory mechanism for hexagonal ordering of the pores has been developed. Ordered pores only occur in Al, and in no other metals to our knowledge. Pores must “migrate” during long-term anodization [21]. We therefore suggest that pore ordering may be a solid-state phenomenon in the barrier layer between the pore bottom and the Al metal, rather than any electrochemical process in the solution above the pore bottoms. Any mutual “repulsion” between pore bottoms will produce pore ordering [23].

#### V. ELECTRODEPOSITION OF Fe AND Co

It is easy to electrodeposit, using alternating current (AC), various metals into the pores of  $\text{Al}_2\text{O}_3$  [6], [12]–[14], [16], [17]. For instance, Co can be electrodeposited by using a sulfate electrolyte ( $\text{CoSO}_4/\text{H}_3\text{BO}_3$ ) [15], and 20 V rms at 200 Hz. Homogeneous nucleation at high current density can be favored by applying a short initial pulse (40–50 V for  $<1$  s), promoting homogeneous growth of nanowires. Filling of the nanometric pores can also be initiated by sonication. Alternating current is needed either because of the rectifying nature of the Al metal/oxide junction, or because of diffusion barriers with the deep nanopores. The lengths of the nanowires can be sampled by transmission electron microscopy (TEM, after dissolving the  $\text{Al}_2\text{O}_3$  matrix away from the  $\alpha$ -Fe in  $\text{H}_2\text{SO}_4/\text{H}_2\text{CrO}_4$  [18], see Fig. 5), by scanning electron microscopy (SEM using back-scattered electrons to maximize atomic number contrast, Fig. 6). If their diameters are known, their average length  $\langle L \rangle$  can be obtained from magnetization data (using the bulk magnetization of  $\alpha$ -Fe or Co), or by measuring the mass gain (Mettler Model AT20 microbalance). Both methods yield a particle length averaged over the sample area. As seen in Fig. 7, there is a distribution of particle lengths for both disordered pores [18] and for ordered pores.

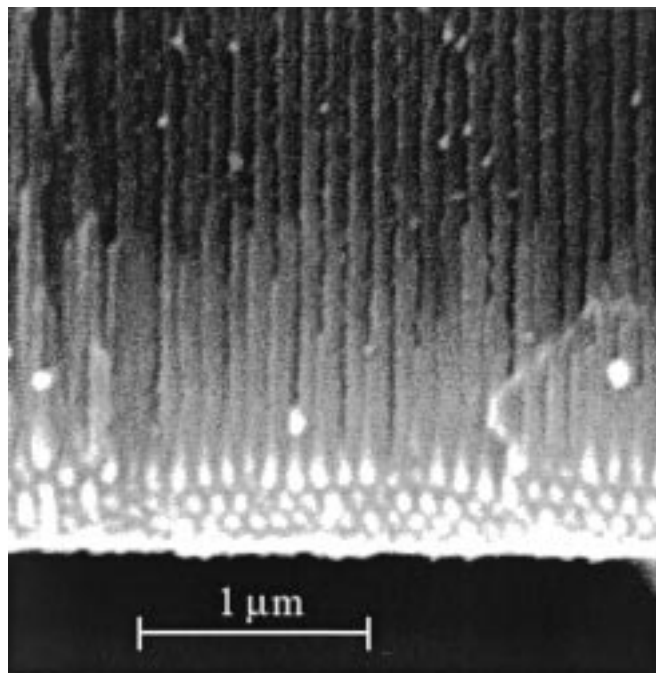


Fig. 6. Cross-sectional SEM image of ordered anodic aluminum oxide partially filled with Co nanowires. Al has been removed with aq.  $\text{HgCl}_2$ .

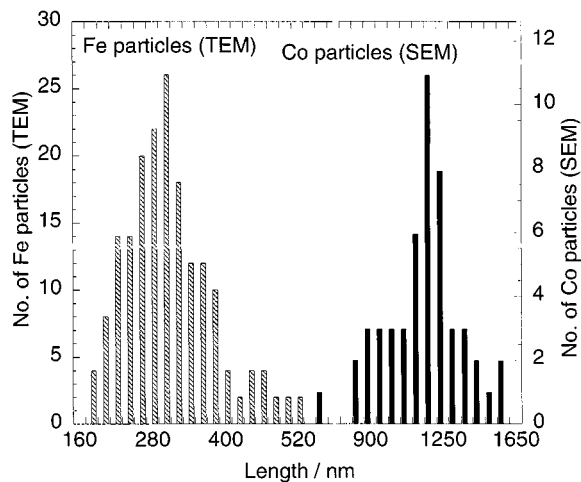


Fig. 7. Distribution of Fe particle lengths (TEM) in disordered alumite (left) [18] and of Co particle lengths (SEM) in ordered alumite (right).

AC electrodeposition from a 0.1 M  $\text{CoSO}_4$ , 0.5 M  $\text{H}_3\text{BO}_3$  solution at 25 V rms and 200 Hz yields nanowires with a hexagonal structure and, for 1  $\mu\text{m}$  nanowires, by X-ray diffraction, a  $(10\bar{1}0)$  orientation, i.e., the crystallographic  $c$ -axis is in-plane, perpendicular to the long direction of the nanowire (Fig. 8). The in-plane orientation is discussed in Section VI.

## VI. MAGNETIC MEASUREMENTS OF Fe AND Co NANOWIRES IN POROUS ALUMINUM OXIDE

In previous work,  $\alpha$ -Fe nanowires were electroplated into approximately hexagonal 11 nm nanopores (Fig. 2) in alumite; the average Fe particle lengths were varied from 200 to 400 nm [18]. The magnetic viscosity was found to be independent of particle length. The measured activation volume was about  $1100 \text{ nm}^3$ ,

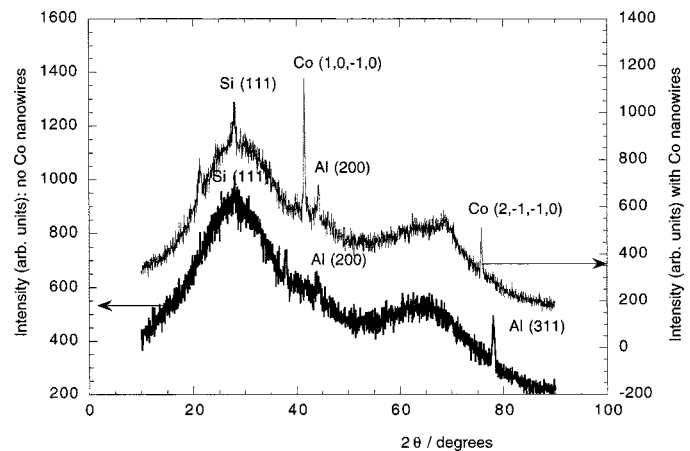


Fig. 8. X-ray powder diffractogram of alumite without Co nanowires (left ordinate) and with Co nanowires (right ordinate).

TABLE I  
MAGNETIC VISCOSITY DATA, NOT CORRECTED FOR DEMAGNETIZING FIELD, FOR LONGER ( $\langle L \rangle = 770 \text{ nm}$ ) AND SHORTER ( $\langle L \rangle = 64 \text{ nm}$ ) Co NANOPARTICLES ELECTRODEPOSITED IN 24.5 nm DIAMETER HEXAGONALLY ORDERED POROUS  $\text{Al}_2\text{O}_3$ : AVERAGE VOLUME  $\langle V \rangle$ , COERCIVITY  $H_c$ , REMANENT COERCIVITY  $H_{cr}$ , PERCENT REMANENT MAGNETIZATION DECAY  $\delta_R$  PER DECADE IN TIME (s), FLUCTUATION FIELD  $H_f$  AND ACTIVATION VOLUME  $V_a$

	Longer (770 nm)		Shorter (64 nm)	
	In-plane	$\perp$ plane	In-plane	$\perp$ plane
$\langle L \rangle / \text{nm}$	770	770	64	64
$\langle V \rangle / (10^3 \text{ nm}^3)$	363	363	30	30
$H_c / \text{Oe}$	313	1912	730	1052
$H_{cr} / \text{Oe}$	1926	1945	1379	1259
$\delta_R (\% / \text{decade})$	0.04	0.98	0.695	1.5
$H_f / \text{Oe}$	N.A.	5.3	8.4	8.4
$V_a / (10^3 \text{ nm}^3)$	N.A.	6.8	4.3	4.3
$V_a / \langle V \rangle$	N.A.	0.02	0.14	0.14

i.e., slightly above the estimated volume for superparamagnetic  $\alpha$ -Fe particles [18].

In the present work, a series of Co nanowires were electroplated into highly ordered alumite porous films. The length was varied by controlling the electroplating time from 30 to 500 s. Magnetic measurements of hysteresis, time-dependent coercivity  $H_c(t)$ , viscosity  $\delta$ , and susceptibility  $\chi$  were made. In every case, the bulk value for Co of the saturation magnetization  $M_s = 1420 \text{ emu cm}^{-3}$  was assumed. The results are summarized in Table I.

Fig. 9(a) shows the out-of-plane and in-plane hysteresis loops for the longer particles with the average length calculated to be  $\langle L \rangle = 770 \text{ nm}$ . The large differences in the remanences show that the easy axis is out-of-plane. The effect of the demagnetizing field  $H_{dz}$ , whose maximum value is 1200 Oe along the  $z$ -axis, is clearly evident in the sheared loop [Fig. 9(a)] and provides a convenient way to estimate the maximum particle diameter. Since  $H_{dz} = 4\pi N_z M_s$ , therefore  $N_z = 0.067$ , which we take to be the average value over the length of the wire. An analytical calculation of  $N_z$  and  $N_x$  for the hexagonal array as a function of the ratio of average particle length  $\langle L \rangle$  to pore spacing  $D_p$  (Fig. 10) shows that  $N_z = 0.067$  corresponds to a

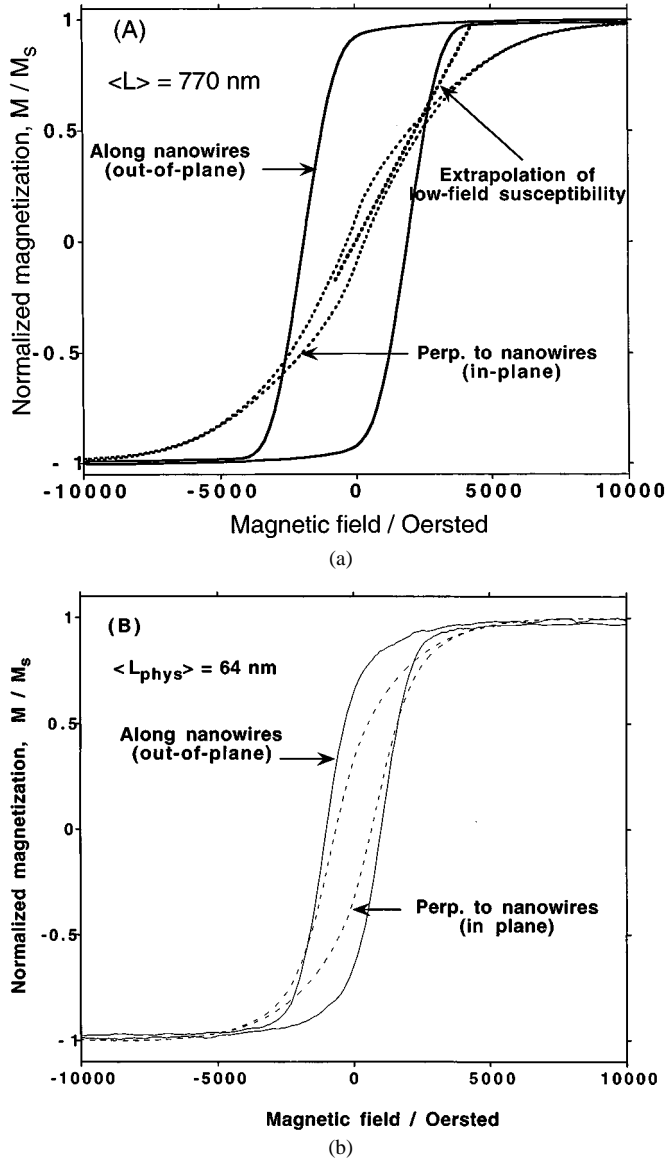


Fig. 9. In-plane (---) and out-of-plane (—) hysteresis loops, of Co nanoparticles with calculated diameter of 24.5 nm, average lengths  $\langle L \rangle = 770$  nm (A: top) and 64 nm (B: bottom). The out-of-plane loops were corrected for the maximum demagnetizing field of 1200 Oe; also shown for the 770 nm particles (A) is the linear extrapolation of the in-plane low-field susceptibility to a total anisotropy field of 4400 Oe.

diameter of 24.5 nm, in reasonable agreement with the AFM estimate of 30 nm (Fig. 3). Taking into account the fractional area coverage  $f = 0.9\langle L \rangle^2/D_p^2$ , the approximate average length of the wires (Table I) was estimated from the saturation moment  $\text{cm}^{-2}$  of the sample. For a cylinder, since  $N_x = N_y = (1 - N_z)/2$ , then using  $N_z = 0.067$  yields  $N_x = N_y = 0.466$ . The shape anisotropy  $K_s = 2\pi(N_x - N_z)M_s^2 = 4.9 \times 10^6 \text{ erg cm}^{-3}$ , resulting in a shape anisotropy field  $H_{K_s} = 2K_s/M_s = 7000$  Oe perpendicular to the wires. Clearly, an anisotropy field of 4400 Oe, obtained by extrapolation of the low-field susceptibility  $\chi$  to saturation [Fig. 9(a)], is much less than the value of 7000 Oe predicted from shape alone. The X-ray data reported above evidenced an in-plane  $c$ -axis in hexagonal Co, and so the associated crystalline anisotropy is the obvious choice to explain the discrepancy. However, the X-ray data alone cannot distin-

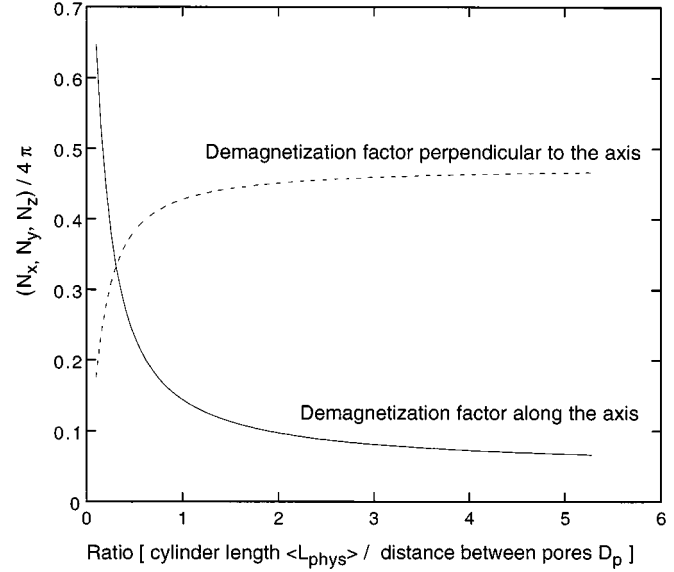


Fig. 10. Average demagnetization coefficients  $N_x = N_y, N_z$  (along the cylinder axis) for a hexagonal array of cylinders of diameter  $D_p = 0.245$  times the distance between cylinders  $D_c$ , as a function of the ratio  $\langle L \rangle/D_c$  of the cylinder length ( $L$ ) to the distance between cylinders  $D_c$ .

guish the relative orientation of the  $c$ -axis in the plane from wire to wire, or within a wire.

If all the  $c$ -axes in all wires were aligned (completely unphysical), and if one assumes for Co an anisotropy constant  $K_1 = 4.0 \times 10^6 \text{ erg cm}^{-3}$ , then the total anisotropy field  $H_{KT}$  would be 1420 Oe, a factor of 3 less than observed. Also, no in-plane anisotropy is observed. A more realistic model is one in which the orientation is uniform in a wire, but varies randomly in direction from wire to wire. We have calculated the initial in-plane susceptibility  $\chi$  for this case, and find

$$\chi = (M_s^2/2K_s)[1 + K_1/2(K_s - K_1)]. \quad (1)$$

For the values assumed above,  $\chi = 0.65$  and  $H_{KT} = 2220$  Oe, still much different than the observed values of 0.32 and 4400 Oe, respectively.

The most likely explanation is that the wires are polycrystalline, with a few grains, each of which has a random in-plane  $c$ -axis. The magnetization, assumed to be uniform within the wire, will average these uniaxial terms. However, because of the finite number of grains, the average will not be zero but will be less than  $K_1$ , and random in direction. Without additional structural data, it is impossible to estimate this effective anisotropy  $K_1^{\text{eff}}$ . From (1), with  $\chi$  equal to the observed value of 0.32, we find  $K_1^{\text{eff}} = 2.9 \times 10^6 \text{ erg cm}^{-3}$ , suggesting relatively few grains in each wire.

The hysteresis loops for the shorter particles are less anisotropic [Fig. 9(b)]. The average length calculated from the magnetic moment is  $\langle L \rangle = 64$  nm, assuming that the Co cross-sectional area, divided by the total surface area, is 24.7%, the same as for the longer particles. The squarenesses are relatively high in both directions, suggesting, because of the “skyline effect,” a mixture of wires with varying lengths, resulting in some with easy axis out-of-plane and some with easy axis in-plane. In fact,  $K_s = K_1^{\text{eff}}$ , when  $(N_x - N_z) = 0.22$ .

From Fig. 10, this corresponds to  $\langle L \rangle = 68$  nm, in good agreement with the experimentally calculated average value.

The remanent viscosity  $\delta_{R||}$ , measured in-plane for the array with  $\langle L \rangle = 770$  nm, was essentially zero, as expected from symmetry. Perpendicular to the plane,  $\delta_{RY}$  was 0.98%/dec. However, it is well known [35] that the intrinsic viscosity  $\delta'_{RY}$  is related to  $4\pi N_z$ , and to the total susceptibility,  $\chi_Y$ , after correcting for the demagnetization field by  $\delta'_{RY} = \delta_{RY}(1 + 4\pi N_z \chi_{RY})$ . However, from Fig. 9(a) it is not possible to determine how much of the slope is due to the demagnetizing field and how much is due to  $\chi'_Y$ . Nevertheless, from the measured values of the remanent viscosity  $\delta_R$  and the irreversible susceptibility  $\chi_{irr}$  the fluctuation field  $H_f = \delta_R/(230\chi_{irr})$  can be calculated, which should be related to the slope of the time-dependent remanent coercivity  $H_{cr}(t)$  versus  $\log t$  at the measurement time. For the longer particles,  $H_f = 5.3$  Oe out-of-plane, and for the shorter particles,  $H_f = 8.4$  Oe in both directions. The larger fluctuation field for the smaller particles is correlated with increased thermal switching.

The activation volume for the Co samples is between  $V_{act} = 4.3 \times 10^3$  nm<sup>3</sup> and  $6.8 \times 10^3$  nm<sup>3</sup>, i.e., well above the superparamagnetic limit for Co. In contrast, a previous study found an activation volume of  $1.1 \times 10^3$  nm<sup>3</sup> for  $\alpha$ -Fe, close to the paramagnetic limit for  $\alpha$ -Fe [18].

## VII. CONCLUSION

Co nanowires can be homogeneously distributed in a controlled fashion over many  $\mu\text{m}^2$  in hexagonally ordered Al<sub>2</sub>O<sub>3</sub> nanopores, but have a distribution of lengths. These systems represent an ideal system for studying time-dependent magnetic phenomena. Theory and experiment provide a convergent view that the Co nanowires studied here ( $\langle L \rangle = 770$  nm or 64 nm, diameter = 24.5 nm), have a distribution of crystallographic *c*-axis orientations in the plane of the film, which are randomized in orientations within the plane, both within a single nanowire and between adjacent nanowires.

## REFERENCES

- [1] S. Charap, P.-L. Lu, and Y. He, "Thermal stability of recorded information at high densities," *IEEE Trans. Magn.*, vol. 33, pp. 978–983, 1997.
- [2] H. N. Bertram and M. Williams, "SNR and density limit estimates: A comparison of longitudinal and perpendicular recording," in *These Proceedings*.
- [3] J. F. Smyth, S. Schultz, D. R. Fredkin, D. P. Kern, S. A. Rishton, H. Schmid, M. Cali, and T. R. Kohler, "Hysteresis in lithographic arrays of permalloy particles: Experiment and theory," *J. Appl. Phys.*, vol. 69, no. 8, pp. 5262–5266, 1991.
- [4] R. M. H. New, R. F. W. Pease, and R. L. White, "Submicron patterning of thin cobalt films for magnetic storage," *J. Vac. Sci. Tech.*, vol. B12, no. 6, pp. 3196–3201, 1994.
- [5] S. Y. Chou, P. R. Krauss, and L. Kong, "Nanolithographically defined magnetic structures and quantum magnetic disk," *J. Appl. Phys.*, vol. 79, no. 8, pp. 6101–6106, 1996.
- [6] N. Tsuya, T. Tokushima, M. Shiraki, Y. Wakui, Y. Saito, H. Nakamura, S. Hayano, A. Furugori, and M. Tanaka, "Alumite disc using anodic oxidation," *IEEE Trans. Magn.*, vol. 22, no. 5, pp. 1140–1144, 1986.
- [7] R. White, R. New, and R. Pease, "Patterned media: A viable route to 50 Gb in<sup>-2</sup> and up for magnetic recording?," *IEEE Trans. Magn.*, vol. 33, pp. 990–995, 1997.

- [8] J. C. Mallinson, "'Transition' and 'statistical' noises in an ideal recording medium," *IEEE Trans. Magn.*, vol. 34, pp. 3816–3817, 1998.
- [9] M. M. Lohrengel, "Thin anodic oxide layers on aluminum and other valve metals: High field regime," *Mater. Sci. Engrg.*, vol. R11, pp. 243–294, 1993.
- [10] F. Keller, M. S. Hunter, and D. L. Robinson, "Structural features of oxide coatings on aluminum," *J. Electrochem. Soc.*, vol. 100, pp. 411–419, 1953.
- [11] G. E. Thompson and G. C. Wood, "Anodic films on aluminum," in *Corrosion: Aqueous Processes and Passive Films—Treatise of Material Science Technology*, J. C. Scully, Ed, New York: Academic Press, 1983, vol. 23, pp. 205–329.
- [12] H. Daimon, O. Kitakami, and H. Fujiwara, "A new method for controlling coercivity of iron deposited alumite films," *J. Magn. Soc. Jpn.*, vol. 13, no. S1, pp. 795–800, 1989.
- [13] C. R. Martin, "Template synthesis of electronically conductive polymer nanostructures," *Acc. Chem. Res.*, vol. 28, pp. 61–68, 1995.
- [14] D. AlMawlawi, N. Coombs, and M. Moskovits, "Magnetic properties of Fe deposited into anodic aluminum oxide pores as a function of particle size," *J. Appl. Phys.*, vol. 70, no. 8, pp. 4421–4425, 1991.
- [15] G. Zangari and D. N. Lambeth, "Porous aluminum oxide templates for nanometer-sized magnetic arrays," *IEEE Trans. Magn.*, vol. 33, no. 5, pp. 3010–3012, 1997.
- [16] X. Bao, F. Li, and R. M. Metzger, "Synthesis and magnetic properties of electrodeposited metal particles on anodic alumite film," *J. Appl. Phys.*, vol. 79, no. 8, pp. 4869–4871, 1996.
- [17] F. Li and R. M. Metzger, "Activation volume of  $\alpha$ -Fe particles in alumite films," *J. Appl. Phys.*, vol. 81, no. 8, pp. 3806–3808, 1997.
- [18] F. Li, R. M. Metzger, and W. D. Doyle, "Influence of particle size on the magnetic viscosity and activation volume of  $\alpha$ -Fe nanowires in alumite films," *IEEE Trans. Magn.*, vol. 33, no. 5, pp. 3715–3717, 1997.
- [19] H. Masuda and K. Fukuda, "Ordered metal nanohole arrays made by a two-step replication of honeycomb structures of anodic alumina," *Science*, vol. 268, pp. 1466–1468, 1995.
- [20] L. Zhang, H. S. Cho, F. Li, R. M. Metzger, and W. D. Doyle, "Cellular growth of highly ordered porous anodic films on aluminum," *J. Mater. Sci. Lett.*, vol. 17, no. 4, pp. 291–294, 1998.
- [21] F. Li, L. Zhang, and R. M. Metzger, "On the growth of highly ordered pores in anodized aluminum oxide," *Chem. Mater.*, vol. 10, no. 9, pp. 2473–2480, 1998.
- [22] O. Jessensky, F. Müller, and U. Gösele, "Self-organized formation of hexagonal pore structures in anodic alumina," *J. Electrochem. Soc.*, vol. 145, pp. 3735–3740, 1998.
- [23] —, "Self-organized formation of hexagonal pore arrays in anodic alumina," *Appl. Phys. Lett.*, vol. 72, pp. 1173–1175, 1998.
- [24] R. E. Ricker, A. E. Miller, D.-F. Yue, G. Banerjee, and S. Bandyopadhyay, "Nanofabrication of a quantum dot array: Atomic force microscopy of electropolished aluminum," *J. Electron. Mater.*, vol. 25, pp. 1585–1592, 1996.
- [25] V. V. Yuzhakov, H.-C. Chang, and A. E. Miller, "Pattern formation during electropolishing," *Phys. Rev.*, vol. B56, pp. 12 608–12624, 1997.
- [26] V. V. Yuzhakov, P. V. Takhistov, A. E. Miller, and H.-C. Chang, "Pattern selection during electropolishing due to double-layer effects," *Chaos*, vol. 9, no. 1, pp. 62–77, 1999.
- [27] V. V. Konovalov, G. Zangari, and R. M. Metzger, "Highly ordered nano-topographies on electropolished aluminum single crystals," *Chem. Mater.*, vol. 11, no. 8, pp. 1949–1951, 1999.
- [28] P. B. Hirsch, "Mosaic structure," in *Progress in Metal Physics*, B. Chalmers and R. King, Eds. London: Pergamon Press, 1956, vol. 6, pp. 236–339.
- [29] J. Randon, P. P. Mardilovich, A. N. Govyadinov, and R. Paterson, "Computer simulation of inorganic membrane morphology: Part 3—Anodic alumina films and membranes," *J. Colloid Interf. Sci.*, vol. 169, pp. 335–341, 1995.
- [30] V. V. Konovalov, unpublished results.
- [31] G. E. Thompson and G. C. Wood, "Anodic films on aluminum," in *Treatise on Materials Science and Technology*, J. C. Scully, Ed, New York: Academic Press, 1983, ch. 5, pp. 205–329.
- [32] V. V. Konovalov and R. M. Metzger, to be published.
- [33] H. Masuda, H. Yamada, M. Satoh, H. Asoh, M. Nakao, and T. Tamamura, "Highly ordered nanochannel-array architecture in anodic alumina," *Appl. Phys. Lett.*, vol. 71, no. 19, pp. 2770–2772, 1997.
- [34] V. P. Parkhutik and V. I. Shershulsky, "Theoretical modeling of porous oxide growth on aluminum," *J. Phys.*, vol. D25, pp. 1258–1263, 1992.
- [35] A. J. Schwartz and W. A. Soffa, "Magnetic viscosity studies of cobalt-aluminum fine-particle measurements," *IEEE Trans. Magn.*, vol. 26, pp. 1816–1820, 1990.